3-21-2012

$Sr_2Fe_{1.5}Mo_{0.5}O_{6-\delta}$ – $Sm_{0.2}Ce_{0.8}O_{1.9}$ Composite Anodes for Intermediate-Temperature Solid Oxide Fuel Cells

Beibei He

Ling Zhao

Shuxiang Song

Tong Liu
University of South Carolina - Columbia, liu348@mailbox.sc.edu

Fanglin Chen
University of South Carolina - Columbia, chenfa@cec.sc.edu

See next page for additional authors

Publication Info

Published in *Journal of The Electrochemical Society*, Volume 159, Issue 5, 2012, pages B619-B626.

Publisher's Version: http://dx.doi.org/10.1149/2.020206jes
He, B., Zhao, L., Song, S., Liu, T., Chen, F., & Xia, C. (21 March 2012). $Sr_2Fe_{1.5}Mo_{0.5}O_{6-\delta}$ – $Sm_{0.2}Ce_{0.8}O_{1.9}$ Composite Anodes for Intermediate-Temperature Solid Oxide Fuel Cells. Journal of The Electrochemical Society, 159 (5), B619 – B626. http://dx.doi.org/10.1149/2.020206jes

Journal of The Electrochemical Society, **159** (5) B619-B626 (2012)
0013-4651/2012/159(5)/B619/8/$28.00 © The Electrochemical Society

$Sr_2Fe_{1.5}Mo_{0.5}O_{6-\delta}$ - $Sm_{0.2}Ce_{0.8}O_{1.9}$ Composite Anodes for Intermediate-Temperature Solid Oxide Fuel Cells

Beibei He,[a] Ling Zhao,[a] Shuxiang Song,[a] Tong Liu,[a] Fanglin Chen,[b,*] and Changrong Xia[a,z]

[a]*CAS Key Laboratory of Materials for Energy Conversion, Department of Materials Science and Engineering, University of Science and Technology of China, Hefei, Anhui 230026, China*
[b]*Department of Mechanical Engineering, University of South Carolina, Columbia, South Carolina 29208, USA*

$Sr_2Fe_{1.5}Mo_{0.5}O_{6-\delta}$ (SFM) perovskite is carefully investigated as an anode material for solid oxide fuel cells with $LaGaO_3$-based electrolytes. Its electronic conductivity under anodic atmosphere is measured with four-probe method while its ionic conductivity is determined with oxygen permeation measurement. Samaria doped ceria (SDC) is incorporated into SFM electrode to improve the anodic performance. A strong relation is observed between SDC addition and polarization losses, suggesting that the internal SFM-SDC contacts are active for H_2 oxidation. The best electrode performance is achieved for the composite with 30 wt% SDC addition, resulting in an interfacial polarization resistance of 0.258 Ω cm^2 at 700°C for $La_{0.8}Sr_{0.2}Ga_{0.8}Mg_{0.2}O_{3-\delta}$ supported single cells. Electrochemical impedance spectroscopy analysis indicates that the high performance of SFM-SDC composite anodes is likely due to the high ionic conductivity and electro-catalytic activity of SDC by promoting the ionic exchange processes. Redox cycle treatment shows that SDC addition can even improve the redox tolerance of SFM anodes.
 [DOI: 10.1149/2.020206jes]

Manuscript submitted January 16, 2012; revised manuscript received February 17, 2012. Published March 21, 2012.

Traditional Ni-based cermets anode has been extensively studied over the years to provide high performance for solid oxide fuel cells (SOFCs). However, Ni is susceptible to degradation by sulfur poisoning, coking, segregation of other impurities at the three-phase boundaries (TPBs), coarsening, and can be severely damaged by reduction-oxidation (redox) cycles due to Ni-NiO phase transitions.[1–4] Ceramic materials offer a number of potential advantages over metals for anode applications, such as mixed ionic-electronic conductivity (MIEC), redox stability and fine microstructures. Many ceramics have thus been investigated as potential anode materials, mainly chromite- and titanate-based perovskites such as $(La_{1-x}Sr_x)_{0.9}Cr_{0.5}Mn_{0.5}O_{3-\delta}$[5,6] perovskite and doped strontium titanium oxides.[7,8] In addition, molybdenum-based double perovskites, which have a general formula of Sr_2MMoO_6 (M = Mg, Fe, Co, and Ni), have been explored as anodes in SOFCs operating with both H_2 and CH_4 fuels.[9–14]

Recently, a novel perovskite $Sr_2Fe_{1.5}Mo_{0.5}O_{6-\delta}$ (SFM) has been reported to show high electrochemical performance as cathode as well as the anode materials for SOFCs.[15–18] However, when SFM alone is used as the anode, the performance is limited. For example, the performance of the fuel cells with SFM anode, $La_{0.8}Sr_{0.2}Ga_{0.83}Mg_{0.17}O_3$ (LSGM) electrolyte and $La_{0.6}Sr_{0.4}Co_{0.2}Fe_{0.8}O_3$ (LSCF) cathode generate peak power density of 0.291 W cm^{-2} at 800°C when wet H_2 is used as the fuel. The power density can be increased significantly when the anode is modified with Ni under the same testing conditions.[18] Ni addition increases the anodic electronic conductivity as well as catalytic activity. In this work, $Sm_{0.2}Ce_{0.8}O_{1.9}$ (SDC) is introduced to enhance the ionic conductivity and catalytic activity so as to increase the anodic activity. SDC is not only a good catalyst for electrochemical redox reaction but also an excellent oxygen ion conductor. The oxygen ion conductivity of SDC at 700°C is 0.041 S cm^{-1}.[19] The introduction of oxygen ion-conducting materials into SOFC electrodes often results in a spatial expansion of the electrochemical reaction zone along the electrode/gas and electrode/electrolyte interfaces, thus reducing the cell polarization losses.[20] Further, the electrochemical reaction kinetics may be improved with SDC since they depend directly on the electrode ionic conductivity, which influences the relative roles of adsorption/desorption as well as charge and mass transfer in the electrode bulk and along the surfaces.[21,22] In addition, the ionic conductivity of SFM is determined with oxygen permeation measurement and the electrical conductivity of SFM-SDC composites in anodic atmosphere is systematically determined.

Experimental

Fuel cell materials preparation and fuel cell fabrication.— The materials used in this work include $Sr_2Fe_{1.5}Mo_{0.5}O_{6-\delta}$ (SFM), $La_{0.8}Sr_{0.2}Ga_{0.8}Mg_{0.2}O_{3-\delta}$ (LSGM), $Sm_{0.5}Sr_{0.5}CoO_3$ (SSC), $Sm_{0.2}Ce_{0.8}O_{1.9}$ (SDC), and CeO_2. SFM powders were synthesized by a glycine-nitrate combustion process.[23] All the starting chemicals have analytical grade, purchased from Sinopharm Chemical Reagent Co., Ltd. $Sr(NO_3)_2$, $Fe(NO_3)_3$ $9H_2O$ and $(NH_4)_6Mo_7O_{24}$ $4H_2O$ were used as the metal precursors. Citric acid was used to adjust the pH value of the solution and to prevent precipitation from hydrolyzation, while glycine was used as the fuel for combustion. After being stirred for several hours, the solution was heated in a microwave oven until self-ignition. The combustion product, dark ashes, was collected and subsequently calcined at 600°C for 2 h and then at 1000°C for 5 h to remove any organic residues to obtain a cubic structure. SSC and SDC powders were also synthesized through the glycine-nitrate process.[23] The LSGM electrolyte powders were synthesized through a citric acid-EDTA process.[24] The crystalline phase study was conducted by X-ray diffraction (XRD, Philips X'pert PROS diffractmeter) analysis using CuKa radiation (D/Max-gA) at room temperature. The microstructure was characterized via a scanning electron microscope (SEM, JSM-6700F, JEOL).

LSGM electrolyte substrates were formed by dry-pressing the LSGM powders into pellets with 15mm in diameter under 300 MPa and then sintered at 1450°C for 5 h to form dense electrolytes. The sintered substrates were about 12 mm in diameter and 0.6 mm thick. For symmetrical cell study, the anode material was applied on both sides of the LSGM electrolyte. An electrode ink consisting of SFM, SDC and terpineol was applied to the LSGM surface using a screen-printing method, and fired at 1000–1200°C in air for 3 h to form porous electrodes. The resulting electrodes were 60 μm thick. Ag slurries were attached to the electrode surface for current collection. LSGM Electrolyte supported single cells with SFM-SDC anodes and SSC-SDC cathodes were fabricated for electrochemical performance and redox stability characterization. SFM-SDC composite anodes were fabricated with the same process as that for the symmetrical cells. SSC-SDC powders with 30 wt% SDC were grounded with 10 wt% ethylcellulose-terpineol binder to make cathode slurry. The slurry was then painted on the other side of the LSGM electrolyte surface and fired at 950°C for 2 h to form the SSC-SDC cathode. The cathode area was 0.238 cm^2. The cell fabrication

*Electrochemical Society Active Member.
zE-mail: xiacr@ustc.edu.cn

process was controlled as consistent as possible so that similar cathodic polarization resistance could be achieved for cells with various anodes.

Oxygen permeation measurements.— The SFM powders were pressed under 200 MPa and sintered at 1400°C in air for 5 h to obtain dense pellets for oxygen permeation measurements. Both sides of the sintered disk were polished and the final thickness was 1.24 mm. After sealed with a glass ring at 1000°C, the membrane has a final effective permeation area of 0.44 cm^2. Oxygen permeation through the SFM dense disk was measured by exposing one side of the disk to the ambient air and sweeping the other side with either helium or carbon monoxide. The effluent was analyzed by an online gas chromatography (1690, KeXiao, China and GC9750, FuLi, China) equipped with a thermal conductivity detector and one column filled with 60–80 mesh GDX-502 for CO_2 detection and the other filled with 60–80 mesh 5A molecular sieves for the other gases detection. The schematic representation of the oxygen-permeation measurement system was described elsewhere.[25]

Electrical conductivity.— Electrical conductivity of the SFM sample was measured using a direct current four-probe method. The pressed green bar was first sintered at 1400°C for 5 h and then reduced at 800°C in wet H_2 (3% H_2O) for 5 h before the conductivity measurement. The electrical conductivity of the porous SFM-SDC composite electrodes was measured by the Van der Pauw method[26,27] from 600 to 800°C. Four Pt contacts (A, B, C, D) were placed on the electrode surface forming an inscribed square in the circular electrode surface to measure two resistances, $R_{AB,CD} = V_{CD}/I_{AB}$, and $R_{BC,DA} = V_{DA}/I_{BC}$ (HP 34401A Digital Multimeter). When difference between the $R_{AB,CD}$ and $R_{BC,DA}$ is small enough, the electrical conductivity (σ) can be obtained with the following Equation

$$\sigma = \frac{\ln 2}{\pi d} \times \frac{2}{R_{AB,CD}+R_{BC,DA}} \quad [1]$$

Where d is the electrode thickness. In the testing configuration, the SFM-SDC composites were applied on one side of the electrolyte with an area of 1.14 cm^2. Pt contacts distance was 0.943 cm and the electrode thickness was about 60 μm.

Electrochemical performance and redox-stability characterization.— Electrochemical measurements were conducted with a Zahner Im6ex electrochemical workstation. Ag paste (DAD-87, Shanghai Research Institute of Synthetic Resins) and Ag wires were used to ensure good electronic contact. The impedance of a symmetrical cell was measured in H_2 (3% H_2O), typically in the frequency range of 1 MHz to 0.01 Hz with signal amplitude of 10 mV over a temperature range of 600–800°C. Area specific polarization resistance, R_p, was determined by the difference of the low and high frequency intercepts of the impedance spectra with the real axis. Single cells were sealed onto alumina tubes with silver paste. Humidified (3% H_2O) hydrogen was used as the fuel with a flow rate of 50 mL min^{-1} and ambient air as the oxidant. The cell current-voltage curve was obtained by using a galvanostatic mode.

Redox tolerance of the SFM-SDC composite anode was measured in single cells with the cell configuration of SFM-SDC |LSGM|SSC-SDC by keeping the cells at 700°C to eliminate the cycling effect. After the cell power density measurement was done but prior to re-oxidation treatment, the anode was first purged with N_2 to displace H_2 fuel and then the anode gas was changed to air. After the SFM-SDC anode was exposed to air for 12 h, the air was again changed to N_2 followed by changing to humidified H_2. Current-voltage curves and impedance spectra were recorded after each redox cycle. A total of four redox cycles have been conducted on the SFM-SDC anode.

Results and Discussion

Electrical and oxygen ionic conductivities of SFM.— XRD analysis shows that a cubic perovskite structure without any impurity has been obtained for the $Sr_2Fe_{1.5}Mo_{0.5}O_{6-\delta}$ (SFM) powders calcined at 1000°C in air for 5 h. The calculated lattice parameter is 7.925(0) Å, which is consistent with the previous report.[15] Upon reduction at 800°C in H_2, SFM shows a perovskite structure with no impurity peak detectable from the XRD studies. Fig. 1a shows the total conductivity measured in reducing atmosphere as a function of temperature. The conductivity increases with the temperature in the range of 400–800°C. Above 600°C, the conductivity increases dramatically, and a

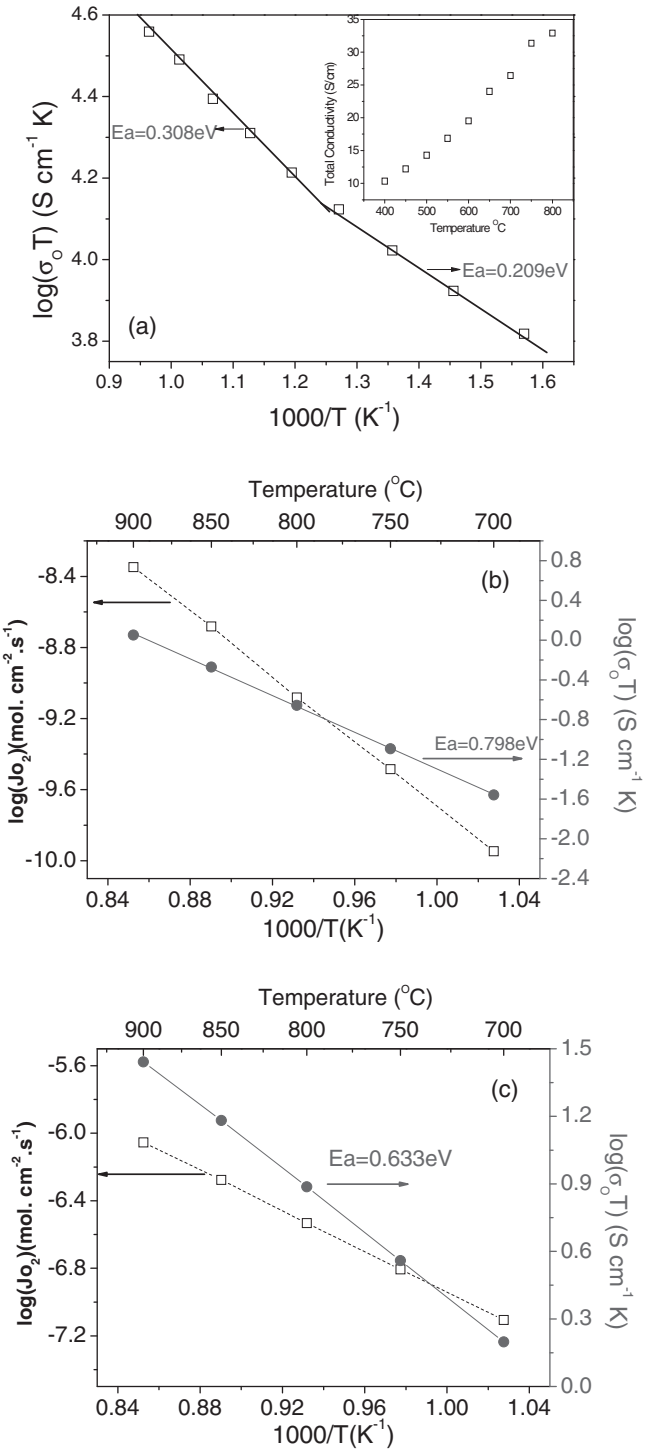

Figure 1. (a) Total conductivity of $Sr_2Fe_{1.5}Mo_{0.5}O_{6-\delta}$ as a function of temperature in wet H_2. (b) Arrhenius plots of oxygen permeation fluxes through $Sr_2Fe_{1.5}Mo_{0.5}O_{6-\delta}$ and the calculated ionic conductivity under air/He gradient and (c) under air/CO gradient.

distinct slope change has been found on the curve. The conductivity enhancement may be attributed to a change in the valence state of Fe and Mo. At elevated temperatures, Fe^{2+} /Mo^{6+} electronic configuration decreases, the contribution of Fe^{3+} /Mo^{5+} increase and result in an increase in the conductivity.[15] At 600°C, the conductivity is 20.9 S cm^{-1}, suggesting that SFM is suitable for anode material of SOFCs operating above 600°C.[28] It is noted that the conductivity is higher than that of $La_{0.75}Sr_{0.25}Cr_{0.5}Mn_{0.5}O_3$ (1.5 S cm^{-1} at 900°C in 5% H_2/Ar) and $Sr_2MgMoO_{6-\delta}$ (9.3 S cm^{-1} at 800°C in H_2), but lower than that of $Sr_{0.86}Y_{0.08}TiO_3$ (82 S cm^{-1} at 800°C and oxygen partial pressure of 10^{-19} atm) and $La_{0.4}Sr_{0.6}TiO_3$ (360 S cm^{-1} at 1000°C and oxygen partial pressure of 10^{-18} atm).[10,29–32]

The oxygen ionic conductivity of SFM is calculated from the oxygen permeation fluxes J_{O2} through a pellet of the thickness L by means of the following Wagner equation

$$\sigma_O = \frac{16F^2 J_{O_2} L}{RTln\left(P_{O_2}^{air}/P_{O_2}^{\text{helium}}\right)} \quad [2]$$

$$\sigma'_O = \frac{16F^2 J_{O_2} L}{RT\ln\left(P_{O_2}^{air}/P_{O_2}^{\text{carbon monoxide}}\right)} \quad [3]$$

Where F is the Faraday's constant, R is the universal gas constant and T is temperature. The difference between the two equations is the oxygen partial of the sweeping gas. Fig. 1b shows the Arrhenius plots of oxygen permeation fluxes through SFM under air/He gradient. It also shows the ionic conductivity calculated with the flux using equation 2. The ionic conductivity under the air/He gradient is relatively small, less than 10^{-3} S cm^{-1} in the temperature range studied. For example, it is 2.06 × 10^{-4} S cm^{-1} at 800°C, a value similar to that of the manganites, but is significantly lower than that of the cobaltites (~ 0.1 S cm^{-1} at 800°C).[33] Fig. 1c shows the temperature dependence of the oxygen permeation rate and the calculated ionic conductivity under air/CO gradient. SFM exhibits higher oxygen permeability and conductivity when the sweep gas is changed to CO. The oxygen ionic conductivity at 800°C ($p_{O2} \approx 10^{-22}$ atm) increases to 0.007 S cm^{-1}, which is one order of magnitude higher than that obtained under the air/He gradient. This might be caused by oxygen vacancy formation associated with Fe^{3+} partial reduction under the reducing atmosphere (Fe^{3+} being partly reduced to Fe^{2+}):

$$2Fe_{Fe}^{x} + O_O^x = 2Fe'_{Fe} + V_O^{\bullet\bullet} + 1/2O_2$$

Therefore, the oxygen ionic conductivity under reducing atmosphere is higher than that in air. The ionic conductivity is beneficial for the anodic reaction, which occurs at the site where oxygen ions are available.

Effect of the SFM anode sintering temperature.— Fig. 2 shows the effect of SFM firing temperature on the electrode performance measured at 800°C in wet H_2 with symmetrical cells. The polarization resistance, R_p, varies significantly with the SFM anode sintering temperature. It can be seen that the R_p is about 0.356 Ω cm^2, the lowest when the electrodes are fired at 1150°C. Sintering temperature below 1100°C might be too low for SFM particles to form good connection and strong bonding with the electrolyte. When the temperature increases from 1150°C to 1200°C, R_p also increases, probably due to the reduction of the electrode porosity and/or the decrease in active SFM surface areas because of the higher anode sintering temperature. Accordingly, an electrode with SFM fired at 1150°C would possess a microstructure that can balance its porosity and adhesion between electrode and electrolyte. Thus in the following sections, 1150°C is used as the sintering temperature for both pure SFM as well as SFM-SDC composite electrodes.

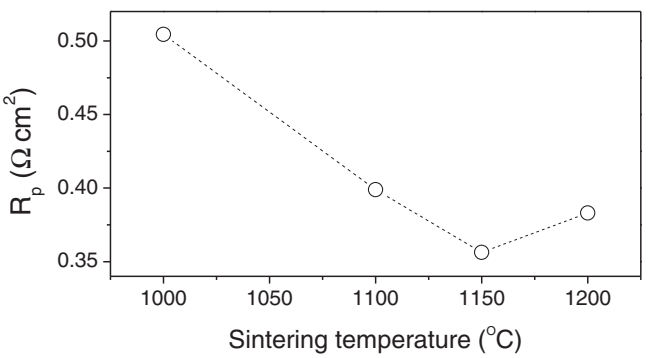

Figure 2. Dependence of the interfacial polarization resistance of pure SFM anode as a function of sintering temperature. The measurement was conducted with symmetrical cells under open circuit conditions in wet H_2.

Effect of SDC addition to SFM on anode performance in symmetrical cells.— Although the ionic conductivity of SFM in anodic atmosphere is higher than that in air, it is still much lower than those of ceria-based electrolytes such as SDC, which is about 0.017 S cm^{-1} at 600°C.[19] It is known that LSGM, SFM and SDC do not react up to 1400°C in air.[15] Therefore, SDC has been incorporated to SFM for form SFM-SDC composite anodes to improve the ionic transport in the anode. However, the total electrical conductivity of SDC is several orders of magnitude lower than that of SFM, even in strongly reducing atmospheres.[34,35] As a result, the addition of SDC in SFM would increase the electrode ionic conductivity while decrease the total electrical conductivity.

The total conductivity has been investigated for porous SFM-SDC electrodes with various SDC contents. Fig. 3 shows their Arrhenius plots for conductivities measured in wet H_2 (~3% H_2O) in the temperature range of 600–800°C. The conductivity decreases gradually with the increase of the SDC content. At 700°C, the total electrical conductivity is 5.21 S cm^{-1} for pure SFM electrode. It drops to 1.42 S cm^{-1} when 30 wt% SDC is added. When the SDC content increases to 50 wt%, the value further reduces to 0.79 S cm^{-1}. Although the total electrical conductivity is reduced while SDC is added, it is still high enough to achieve reasonable cell performance. For example, for a 60 μm thick anode, a conductivity of 0.79 S cm^{-1} results in an area specific resistance of 0.006 Ω cm^2, which is negligible to the total cell resistance typically observed for an operating fuel cell.[36] Consequently the electrical conductivity of the SFM-SDC anodes is still high enough to achieve acceptable cell performance at intermediate temperatures.

Impedance spectra for SFM electrodes with various SDC contents are measured with a symmetrical cell configuration in wet H_2 (~3% H_2O). Fig. 4a is the effect of SDC addition on R_p for these electrodes

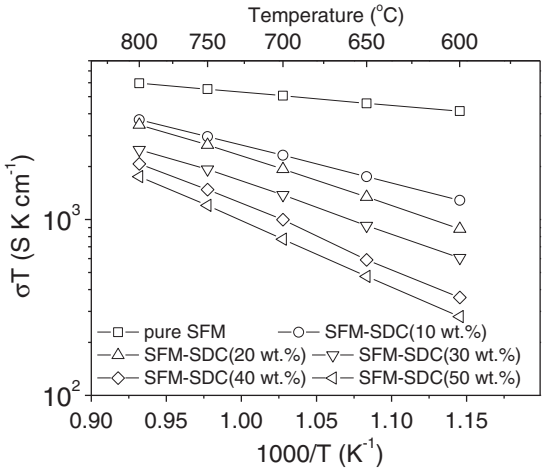

Figure 3. Electrical conductivities of the porous SFM-SDC composite anodes with various SDC amount.

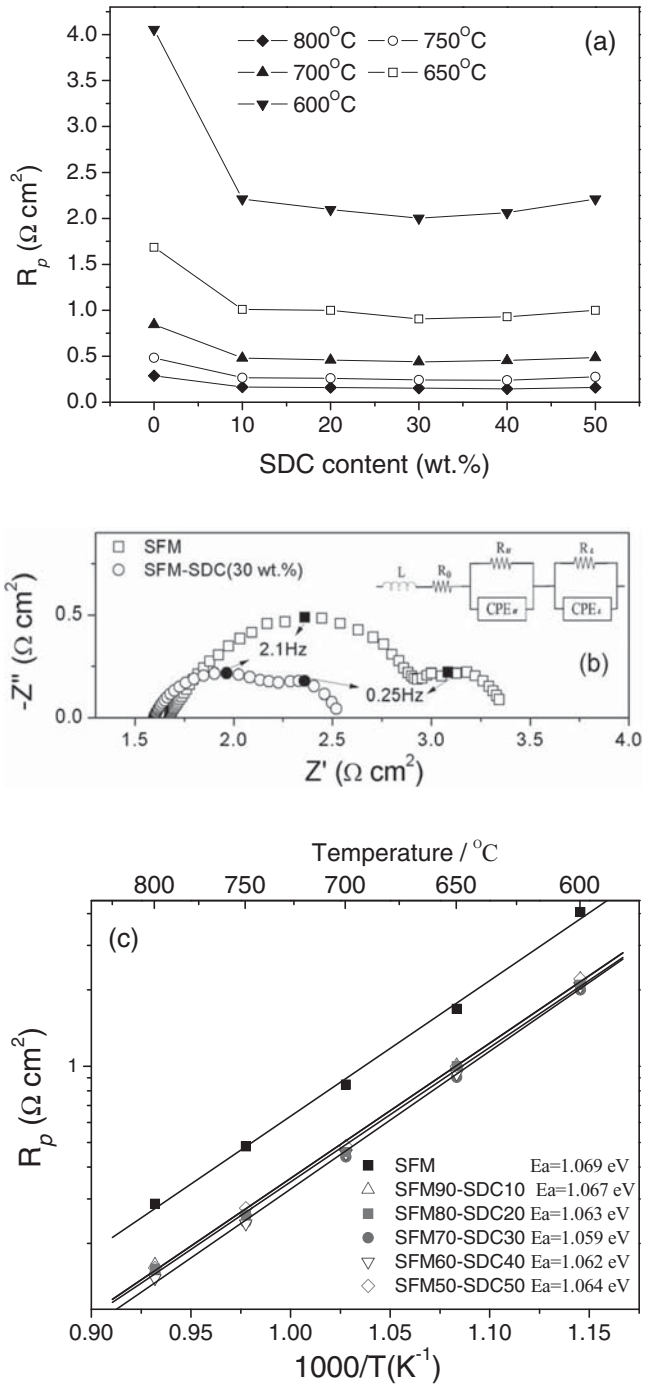

Figure 4. (a) Dependence of interfacial polarization resistance for electrodes with various SDC amount in composite anodes as a function of temperature in wet H_2. (b) Impedance spectra of the cells with pure SFM and SFM-SDC (30 wt%) anodes measured under open circuit conditions at 700°C. (c) The slope of the curve in the Arrhenius plots.

on LSGM electrolytes at 600–800°C. SDC addition has significant effect on reducing R_p. In the range of 0∼30 wt%, more SDC addition results in smaller R_p. For example, R_p at 700°C of the pure SFM electrode is 0.84 Ω cm^2. It decreases to 0.48 Ω cm^2 with 10 wt% SDC addition; and further to 0.45 Ω cm^2, about only half of that for pure SFM, when 30 wt% SDC is added, indicating that the electrode performance is substantially improved by incorporating SDC into SFM. Adding SDC would significantly extend the triple phase boundaries for the electrochemical oxidation reaction of the fuel, and consequently reduce the electrode polarization resistance. Further addition of SDC (40–50 wt%) results in slightly increase of R_p, which might be caused by the decrease of electrochemical reaction sites with the decrease of SFM, and/or the blockage of the electronic seepage channel of SFM by a large amount of SDC.

Fig. 4b shows the impedance spectra at 700°C for the symmetrical cells with the pure SFM and SFM with SDC (30 wt%) composite electrode. The impedance spectra consist of two arcs. The high frequency impedance responses are likely related to the ionic exchange processes, while the low frequency impedance to the non-charge processes including oxygen surface exchange and diffusion reactions.[37,38] To identify these steps, equivalent circuit, $LR_0(R_HCPE_H)(R_LCPE_L)$, is applied to fit the impedance spectra using Zview program. The pure SFM electrode presents a larger high-frequency arc than the low frequency one. The resistance associated with the high frequency process, $R_H = 1.328$ Ω cm^2, is much larger than the resistance with the low frequency process, $R_L = 0.325$ Ω cm^2. The result suggests that the polarization of pure SFM electrode is dominated by the ionic transfer process. When 30 wt% SDC is added, the impedance responses at high frequency decreases significantly, and R_H is only 0.639 Ω cm^2. The substantial decrease in high frequency resistance clearly demonstrates that adding SDC in SFM can significantly improve the ionic exchange kinetics of the SFM anodes. It is noted that the impedance responses at low frequency also slightly decreases when SDC is added, R_L = 0.282 Ω cm^2, very close to that of pure SFM electrode. Thus, the addition of SDC not only promotes the O^{2-} incorporation process at the interface between electrolyte and SFM-SDC anode, but also the O^{2-} transport in the anode bulk, consequently enhancing the electrochemical oxidation reaction. Similar results are also obtained when gadolinium-doped ceria is incorporated with LSCM anodes.[39]

Another evidence for the increased O^{2-} incorporation rate is the calculated pseudo capacitance C_H of R_HCPE_H. For the pure SFM electrode, the corresponding pseudo capacitance, C_H, is about 0.0103 F cm^{-2}. When 30 wt% SDC is added, it increases by a factor of 4 to about 0.0378 F cm^{-2}. The high frequency process links with the TPB, larger capacitance indicates larger TPB area, and larger TPB area means more parallel O^{2-} incorporation paths.[40,41]

According to the binary-random-sphere packing model and percolation theory, the maximum TPB length is a function of the two phase composition and particle size ratio of electronic to oxygen ionic conductors.[42] When the two phase particles have the same size, the maximum TPB length is obtained at the content of equal volume fraction; when the particle size of the ionic phase is smaller than the electronic phase, the maximum TPB length is obtained at the content with the volume fraction of the ionic conductor less than 50%. For the optimized composition with 30 wt%SDC, the volume fraction of SDC is 28%. The results are consistent with the theoretical prediction since the particle size of SDC is smaller than SFM, which can be seen from the SEM images (Fig. 5).

Fig. 4c shows that the slope of the curve in the Arrhenius plots is very close to each other for all the SFM-SDC composite anodes. Therefore, SDC addition has negligible effect on the activation energy, suggesting that introducing SDC into the SFM anodes does not significantly change the mechanism of the electrochemical oxidation of hydrogen.

The electrochemical performance depends critically on the electrode microstructure.[43,44] Fig. 5 presents the SEM micrographs of the SFM-SDC composites with various compositions. For pure SFM, the particle size is in the range of 1–2 μm (Fig. 5a). When 10 wt% SDC is added, the microstructure does not change obviously. Small SDC particles present clearly when SDC content increases to 30 wt%. Further addition of SDC (50 wt%) results in increased porosity (Fig. 5d). This may be caused by the reduced grain growth of the SFM phase due to the inhibiting effect of SDC phases. The microstructure is also characterized by large SFM particles embedded in fine SDC particles. Consequently, the connectivity of SFM gradually reduces with the increase of SDC content, leading to reduced electronic conductivity (Fig. 3). The microstructure change might also explain the increased value of R_p for the SFM-SDC composites with 50 wt% SDC (Fig. 4).

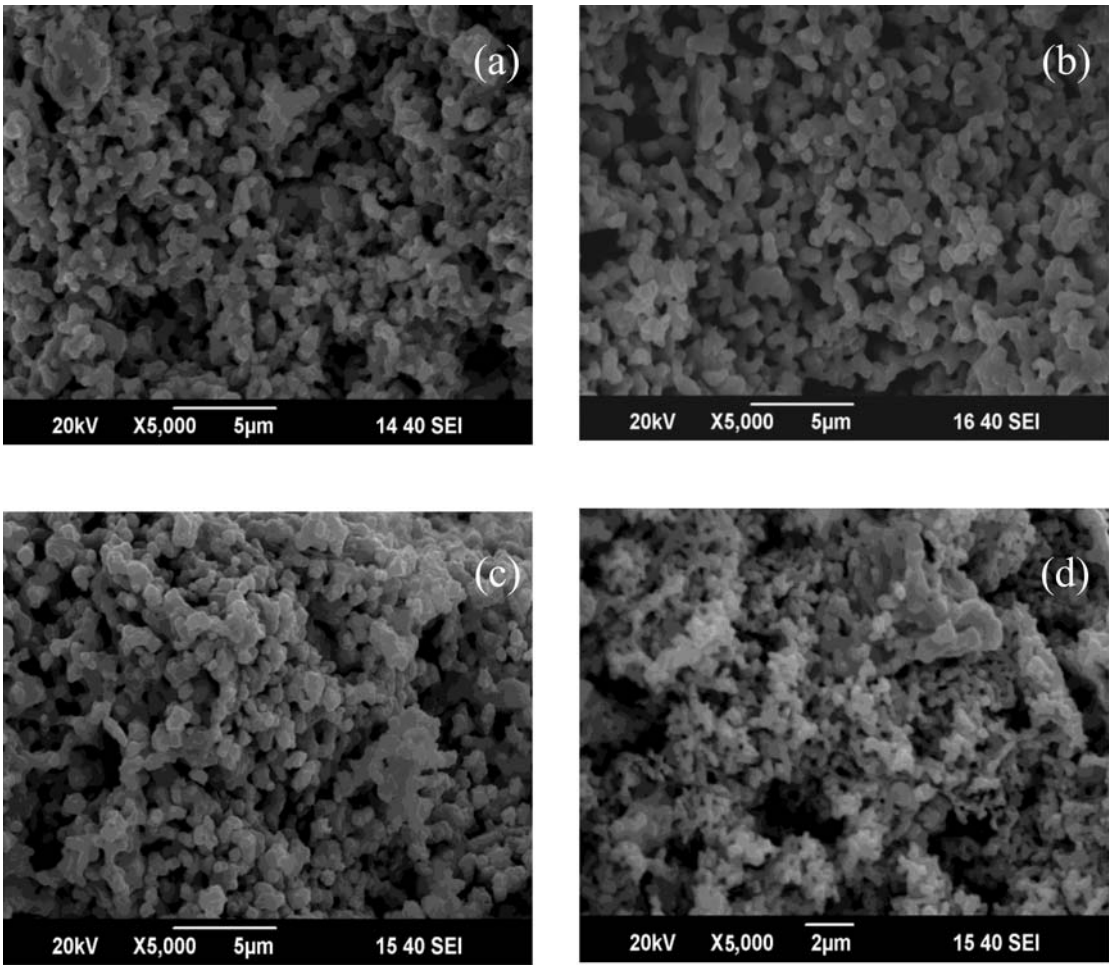

Figure 5. SEM micrographs of cross-sectional views of (a) pure SFM, (b) SFM (90 wt%)-SDC (10 wt%), (c) SFM (70 wt%)-SDC (30 wt%) and (d) SFM (50 wt%)-SDC (50 wt%) anodes.

Effect of SDC addition to SFM anode on single cells performance.— The effect of SDC cooperation is further investigated with single cells consisting of SFM-SDC anodes, LSGM electrolytes, and SSC-SDC cathodes. Fig. 6 shows the peak power density of these cells using SFM-SDC composite anodes with various SDC contents. The power density changes with the SDC content, indicating that the anodic activity varies with the composition since the electrolytes and cathodes are the same for these cells. The highest power density is achieved with 30–40 wt% SDC addition. This generally agrees with the result for interfacial polarization resistance obtained with symmetrical cells shown in Fig. 4. With SFM-SDC (30 wt%) composite anodes, the peak power density at 700°C is 279 mW cm^{-2}. The LSGM electrolyte used in the single cell testing is around 600 μm. The cell power density is expected to be substantially improved if the electrolyte thickness is further reduced according to the cell performance shown in Fig. 7.

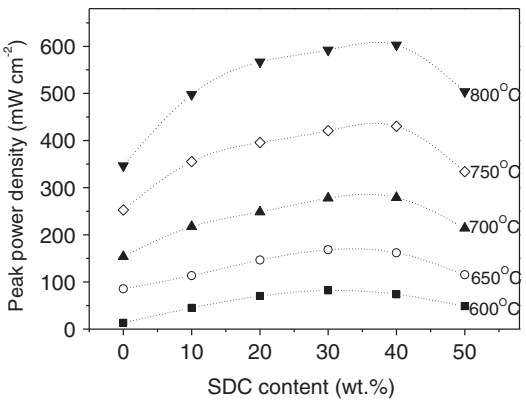

Figure 6. Maximum cell power densities of single cells using SFM-SDC composite anodes as a function of SDC amount in the composite anodes.

In addition to providing ionic conductivity, ceria can also enhance the electrode performance by providing catalytic activity[45,46] since ceria is an excellent oxidation catalyst widely used in this role in automotive three-way catalysis.[47,48] To examine the role of SDC more closely, CeO_2 and LSGM are added to SFM to form composite anodes, both having 30 wt% oxide additions. Fig. 7a shows the cell power density of single cells using hydrogen as the fuel. Single cells with SFM-CeO_2, SFM-SDC and SFM-LSGM composite anodes produce peak cell power densities of 197, 272 and 166 mW cm^{-2} at 700°C, respectively. The corresponding interfacial polarization resistances under open-circuit conditions are 0.458, 0.338 and 0.562 Ω cm^2, respectively, as shown in Fig. 7b. Compared with cells using SFM-CeO_2 and SFM-LSGM anodes, the cell with SFM-SDC anode exhibits smaller arcs for interfacial polarization resistance. Since the three cells have the same electrolytes and cathodes, the differences in the cell impedance spectra may be attributed to the anodes. At 700°C, the conductivity of LSGM is similar to that of SDC,[49] but LSGM is not catalytically active for hydrogen reduction. Although CeO_2 is also highly electro-catalytically active, its ionic conductivity is much lower than that of SDC, even in the reducing

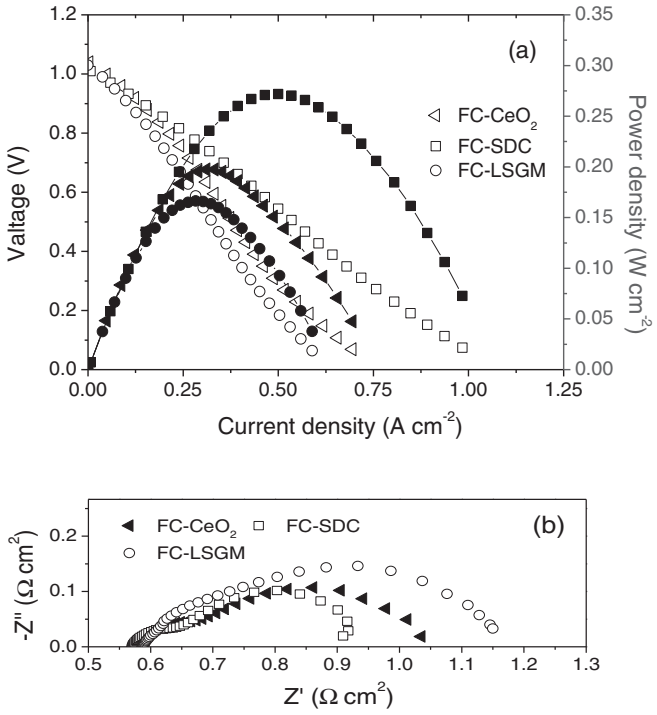

Figure 7. (a) Typical *I–V* and *I–P* curves measured at 700°C for single cells based on SFM-CeO_2, SFM-SDC and SFM-LSGM composite anodes with humidified H_2 as the fuel and ambient air as the oxidant and (b) impedance spectra of single cells measured under open circuit conditions.

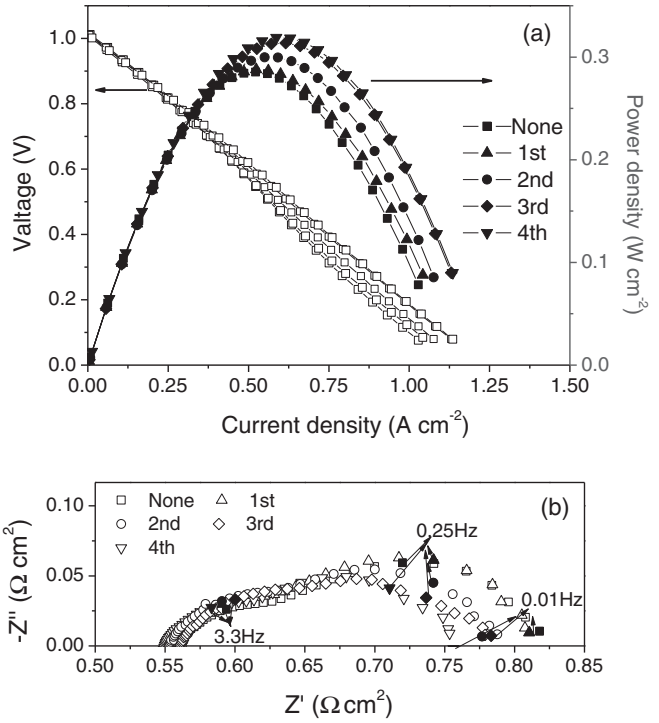

Figure 8. (a) *I–V* and *I–P* curves measured at 700°C for the single cells using SFM -SDC (30 wt%) as composite anodes after exposure to air showing changes over 4 redox cycles and (b) impedance spectra measured under open circuit conditions.

atmosphere. Among these three oxides, SDC has the properties of high catalytic activity and oxide ionic conductivity, therefore, cells with SFM-SDC anodes show the lowest interfacial polarization resistance and highest power density. This also agrees with those obtained in previous studies in which the use of acceptor-doped cerium dioxide exhibits a significant mixed ionic-electronic conductivity under reducing conditions,[50,51] and demonstrates better performance compared to the undoped CeO_2.[52]

Redox tolerance of SFM-SDC composite anodes.— In contrast to cermets anode such as Ni-based cermets, an advantage of oxide anode is the tolerance against redox cycling. Therefore, oxidation tolerance of the SFM-SDC (30 wt%) composite anode is examined. Since this work focuses on intermediate temperature operation, redox cycle is conducted at 700°C. Fig. 8a shows the performance of the fuel cells after the redox cycles. In contrast to Ni cermet anode, which is permanently damaged after re-oxidation treatment, evidently, the power density of the cell does not decrease, but slightly increases by oxidation treatment. The redox performance is further studied using electrochemical impedance spectroscopy. Fig. 8b shows the impedance plots of single cells before and after redox treatment. It is also noted that the ohmic resistance (R_Ω) is slightly decreased. The R_Ω value is 0.560 Ω cm^2 for the fresh cell, and reduces to 0.550 Ω cm^2 after four redox cycles. The interfacial polarization resistance at 700°C is 0.263 Ω cm^2 for the fresh cell but decreases to 0.206 Ω cm^2 after four redox cycles.

As there might be the formation of new compounds during the redox cycling, which might be active to the anode reaction leading to reduced interfacial polarization resistances, XRD measurement is performed on the SFM-SDC anodes before and after the redox treatment. It can be seen in Fig. 9 that the XRD patterns of the SFM-SDC anodes are basically the same and no secondary phases are observable during the redox treatment, suggesting good chemical compatibility of SFM with SDC in the anodic atmosphere under the fuel cell operating conditions. Since new compounds are not formed, the improved cell performance might be the caused by the activation polarization of the freshly prepared SSC cathode. The cathode activation effect has been found with typical cathodes, which can be significantly activated with current passing and result in much smaller interfacial polarization resistance.[53] Consequently, cathodic activation might be one of the reasons for the improved cell performance observed during the redox cycling.

It is generally known that reduction leads to the volume expansion, so volume change is reasonably expected for SFM-SDC composite anode during redox treatment. It has been reported that $(La_{0.75}Sr_{0.25})Cr_{0.5}Mn_{0.5}O_{3-\delta}$ anode can dramatically change microstructure from filmlike dense structure to porous structure with

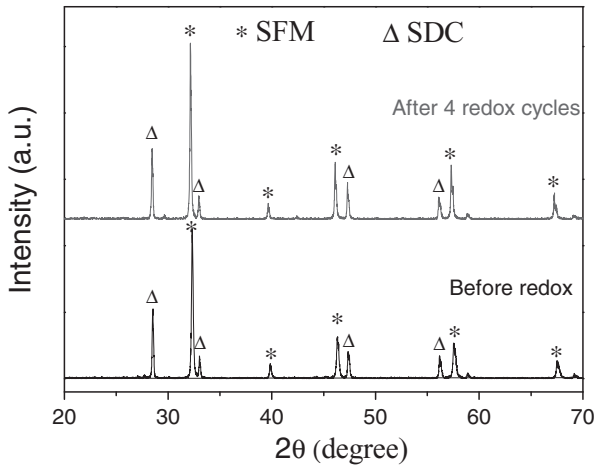

Figure 9. XRD patterns of SFM-SDC (30 wt%) composite anodes on LSGM electrolyte before and after redox treatment.

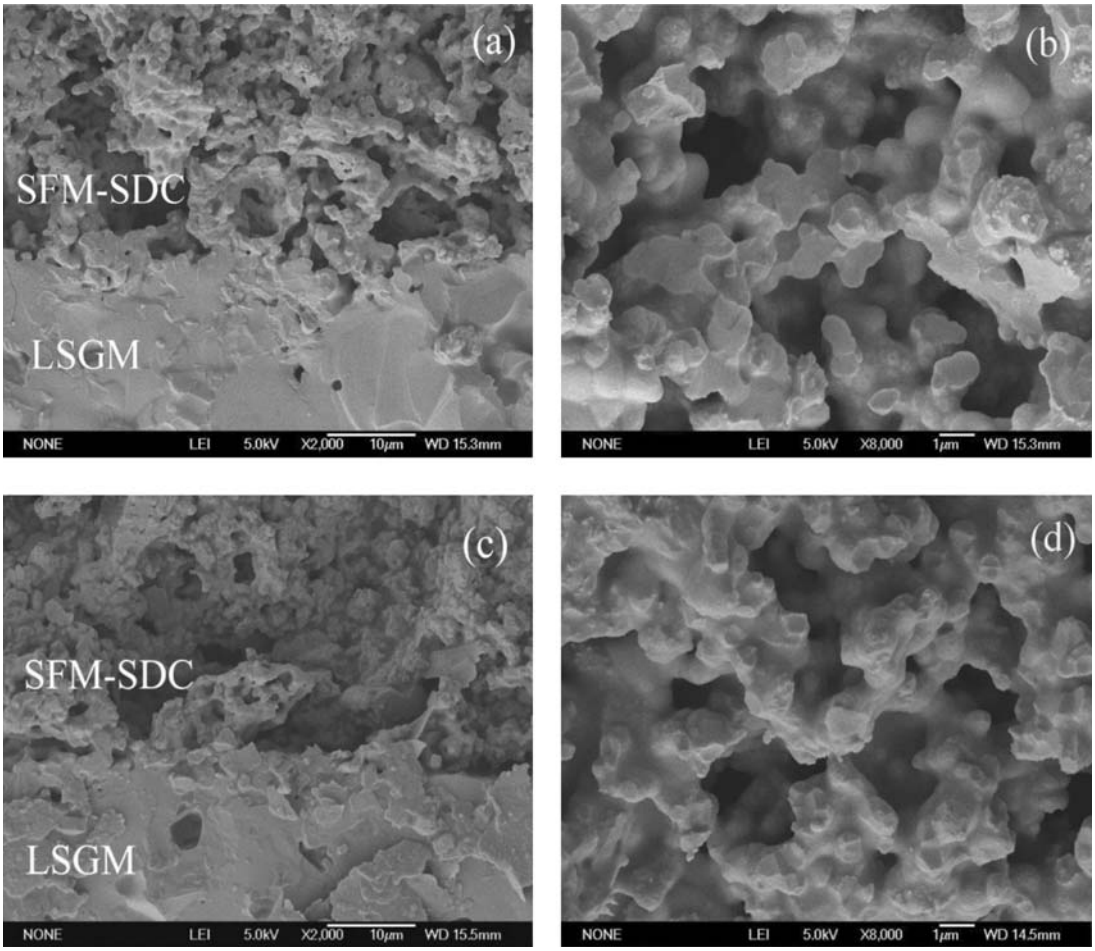

Figure 10. Cross-sectional views of LSGM-electrolyte and SFM-SDC (30 wt%) composite anodes before and after redox cycle. (a) anode and electrolyte interface cross section before redox cycle, (b) high magnification SEM images of anodes before redox cycle; (c) anode and electrolyte interface cross section after the forth re-oxidation cycle, (d) high magnification SEM images of anodes after the forth re-oxidation cycle.

very small particles by redox cycles.[54] The morphologic modification of the anode surface with redox cycle would suggest a change in lattice volume caused by a mixed valence state of Mn and Fe. Therefore, a similar broken surface of SFM-SDC anode is also expected as the results of Fe^{2+} /Mo^{6+} and Fe^{3+}/Mo^{5+} variation. XRD analysis shows that there is a change to the size of the cubic structure, from a = 7.925(0) Å in air to a = 7.928(4) Å in anodic atmosphere. The partial reduction, $Ce^{4+} \rightarrow Ce^{3+}$ in SDC might also cause microstructure change. Fig. 10 shows the change in the microstructure of SFM-SDC (30 wt%) composite anode before and after redox cycling. Evidently, the surface morphology of the particle changes but the particle size keeps unchanged. Delamination is not observed between the anode and electrolyte after four redox cycles. Consequently, SFM-SDC (30 wt%) composites demonstrate high activity to the anode reaction but also are stable against redox cycling.

Conclusions

SFM is examined as an anode material for LSGM electrolyte supported intermediate temperature SOFCs. In anodic atmosphere of humidified H_2, SFM has a total conductivity of 20.9 S cm^{-1} at 600°C. Its oxygen ionic conductivity is relatively low. SDC is thus incorporated to increase its anodic performance. Adding SDC has substantially increased the TPB as well as electrode catalytic activity, and reduced the interfacial polarization resistance, from 0.84 Ω cm^2 to 0.45 Ω cm^2 at 700°C when 30 wt% SDC is added. In addition, higher cell power density and smaller cell interfacial polarization resistance have been achieved in single cells using SFM-SDC (30 wt%) anodes compared with those using pure SFM anodes. Furthermore, this study has demonstrated that the SFM-SDC composite anodes are highly tolerant against redox cycling. Consequently, SFM-SDC composite are highly promising ceramic anodes for intermediate temperature SOFCs.

Acknowledgment

We gratefully acknowledge the financial support from the Ministry of Science and Technology of China (2012CB215403) and the HeteroFoaM Center, an Energy Frontier Research Center funded by the US Department of Energy Office of Science, Office of Basic Energy Sciences under Award Number DE-SC0001061.

References

1. B. C. H. Steele, I. Kelly, H. Middleton, and R. Rudkin, *Solid State Ionics*, **28–30**, 1547 (1988).
2. M. Y. Gong, X. B. Liu, J. Trembly, and C. Johnson, *J. Power Sources*, **168**, 89 (2007).
3. L. Yang, S. Z. Wang, K. Blinn, M. F. Liu, Z. Liu, Z. Cheng, and M. L. Liu, *Science* **326**, 126 (2009).
4. S. W. Tao and J. T. S. Irvine, *Adv. Mater.*, **17**, 1734 (2005).
5. S. W. Tao and J. T. S. Irvine, *Nat. Mater.* **2**, 320 (2003)
6. D. M. Bastidas, S. W. Tao, and J. T. S. Irvine, *J. Mater. Chem.*, **16**, 1603 (2006).
7. O. A. Marina, N. L. Canfield, and J. W. Stevenson, *Solid State Ionics*, **149**, 21 (2002).
8. S. Q. Hui and A. Petric, *J. Electrochem. Soc.*, **149**, J1 (2002).
9. Y. H. Huang, R. I. Dass, J. C. Denyszyn, and J. B. Goodenough, *J. Electrochem. Soc.*, **153**, A1266 (2006).

10. Y. H. Huang, R. I. Dass, Z. L. Xing, and J. B. Goodenough, *Science*, **312**, 254 (2006).
11. Y. H. Huang, G. Liang, M. Croft, M. Lehtimaki, M. Karppinen, and J. B. Goodenough, *Chem. Mater.* **21**, 2319 (2009).
12. C. Graves, B. R Sudireddy, and M. Mogensen, *ECS Trans.*, **28**, 173 (2010).
13. S. Colis, D. Stoeffler, C. Mény, T. Fix, C. Leuvrey, G. Pourroy, A. Dinia, and P. Panissod, *J. Applied physics*, **98**, 033905 (2005).
14. Z. M. Wang, Y. Tian, and Y. D. Li, *J. Power Sources*, **196**, 6104 (2011).
15. Q. Liu, X. Dong, G. Xiao, F. Zhao, and F. Chen, *Adv. Mater.*, **22**, 5478 (2010).
16. G. Xiao, Q. Liu, F. Zhao, L. Zhang, C. R. Xia, and F. Chen, *J. Electrochem. Soc.*, **158**, B455 (2011).
17. L. Zhang, Y. Q. Liu, Y. X. Zhang, G. L. Xiao, F. L. Chen, and C. R. Xia, *Electrochem. Commun.*, **13**, 711 (2011).
18. G. L. Xiao and F. L. Chen, *Electrochem. Commun.*, **13**, 57 (2011).
19. H. Yahiro, K. Eguchi, and H. Arai, *Solid State Ionics*, **36**, 71 (1989).
20. S. B. Adler, *Solid State Ionics*, **111**, 125 (1998).
21. M. L. Liu, *J. Electrochem. Soc.*, **145**, 142 (1998).
22. J. Fleig and J. Maier, *J. Eur. Ceram. Soc.*, **24**, 1343 (2004).
23. C. R. Xia, W. Rauch, F. Chen, and M. L. Liu, *Solid State Ionics*, **149**, 11 (2002).
24. W. B. Wang, Z. J. Yang, H. T. Wang, G. L. Ma,, W. J. Gao, and Z. F. Zhou, *J. Power Sources*, **196**, 3539 (2011).
25. K. Wu, S. Xie, G. S. Jiang, W. Liu, and C. S. Chen, *J. Membrane Science*, **188**, 189 (2001).
26. L. J. van der PAUW, *Philips Res. Rep.*, **13**, 1 (1958).
27. A. Esquirol, N. P. Brandon, J. A. Kilner, and M. Mogensen, *J. Electrochem. Soc.*, **151**, A1847 (2004).
28. A. Atkinson, S. Barnett, R. J. Gorte, J. T. S. Irvine, J. Mcevoy, M. Mogensen, S. C. Singhal, and J. Vohs, *Nat. Mater.*, **3**, 17 (2004).
29. G. Kim, G. Corre, J. T. S. Irvine, J. M. Vohs, and R. J. Gorte, *Electrochem. Solid State Lett.*, **11**, B16 (2008).
30. D. Marrero-Lo/pez, J. Pena-Martnez, J. C. Ruiz-Morales, D. Perez-Coll, M. A. G. Aranda, and P. Nunez, *Mater. Res. Bull.*, **43**, 2441 (2008).
31. S. Q. Hui and A. Petric, *J. Electrochem. Soc.*, **149**, J1 (2002).
32. O. A. Marina, N. L. Canfield, and J. W. Stevenson, *Solid State Ionics*, **149**, 21 (2002).
33. E. V. Tsipis and V. V. Kharton, *J. Solid State Electrochem.*, **12**, 1039 (2008).
34. H. Inaba and H. Tagawa, *Solid State Ionics*, **83**, 1 (1996).
35. D. Ding, B. B. Liu, Z. N. Zhu, S. Zhou, and C. R. Xia, *Solid State Ionics*, **179**, 896 (2008).
36. Z. Y. Jiang, C. R. Xia, F. Zhao, and F. L. Chen. *Electrochem. Solid State Lett.*, **12**, B91 (2009).
37. S. B. Adler, J. A. Lane, and B. C. H. Steele, *J. Electrochem. Soc.*, **143**, 3554 (1996).
38. S. B. Alder, *Solid State Ionics*, **135**, 603 (2000).
39. S. P. Jiang, X. J. Chen, S. H. Chan, and J. T. Kwok, *J. Electrochem. Soc.*, **153**, A850 (2006).
40. R. Chiba, T. Komatsu, H. Orui, H. Taguchi, K. Nozawa, and H. Arai, *Electrochem. Solid State Lett.*, **12**, B69 (2009).
41. Z. Y. Jiang, L. Zhang, K. Feng, and C. R. Xia, *J. Power Sources*, **185**, 40 (2008).
42. X. J. Chen, S. H. Chan, and K. A. Khor, *Electrochim. Acta*, **49**, 1851 (2004).
43. M. Brown, S. Primdahl, and M. Mogensen, *J. Electrochem. Soc.*, **147**, 475 (2000).
44. T. Suzuki, Z. Hasan, Y. Funahashi, T. Yamaguchi, Y. Fujishiro, and M. Awano, *Science*, **325**, 852 (2009).
45. S. McIntosh, J. M. Vohs, and R. J. Gorte, *Electrochim. Acta*, **47**, 3815 (2002).
46. S. Zhao and R. J. Gorte, *Appl. Catal. A*, **248**, 9 (2003).
47. R. J. Gorte, *AIChE Journal*, **56**, 1126 (2010).
48. E. Aneggi, M. Boaro, C. de Leitenburg, G. Dolcetti, and A. Trovarelli, *J. Alloys Compd.*, **408**, 1096 (2006).
49. S. M. Haile, *Acta Materialia*, **51**, 5981 (2003).
50. B. Dalslet, P. Blennow, P. V. Hendriksen, N. Bonanos, D. Lybye, and M. Mogensen, *J. Solid State Electrochem.*, **10**, 547 (2006).
51. V. V. Kharton, F. M. Figueiredo, L. Navarro, E. N. Naumovich, A. V. Kovalevsky, A. A. Yaremchenko, A. P. Viskup, A. Carneiro, F. M. B. Marques, and J. R. Frade, *J. Mater. Sci.*, **36**, 1105 (2001).
52. S. P. Jiang, Y. Y. Duan, and J. G. Love, *J. Electrochem. Soc.*, **149**, A1175 (2002).
53. W. Wang and S. P. Jiang, *J. Solid State Electrochem.*, **8**, 914 (2004).
54. G. Kim, S. Lee, J. Y. Shin, G. Corre, J. T. Irvine, J. M. Vohs, and R. J. Gorte, *Electrochem. Solid State Lett.*, **12**, B48 (2009).